Hearing Research 322 (2015) 235–241

Contents lists available at ScienceDirect

Hearing Research

journal homepage: www.elsevier.com/locate/heares

Superior temporal resolution of Chronos versus channelrhodopsin-2 in an optogenetic model of the auditory brainstem implant

Ariel Edward Hight [a, c, 1], Elliott D. Kozin [a, b, 1], Keith Darrow [d], Ashton Lehmann [a, b], Edward Boyden [e], M. Christian Brown [a, b], Daniel J. Lee [a, b, *]

[a] Eaton-Peabody Laboratories, Massachusetts Eye and Ear Infirmary, Boston, MA, USA
[b] Department of Otology and Laryngology, Harvard Medical School, Boston, MA, USA
[c] Program in Speech and Hearing Bioscience and Technology, Harvard Medical School, Boston, MA, USA
[d] Department of Communication Sciences and Disorders, Worcester State University, Worcester, MA, USA
[e] Departments of Brain and Cognitive Sciences and Biological Engineering, MIT Media Lab and McGovern Institute, MIT, Cambridge, MA, USA

ARTICLE INFO

Article history:
Received 20 August 2014
Received in revised form
6 November 2014
Accepted 8 January 2015
Available online 15 January 2015

ABSTRACT

Contemporary auditory brainstem implant (ABI) performance is limited by reliance on electrical neurostimulation with its accompanying channel cross talk and current spread to non-auditory neurons. A new generation ABI based on optogenetic technology may ameliorate limitations fundamental to electrical stimulation. The most widely studied opsin is channelrhodopsin-2 (ChR2); however, its relatively slow kinetic properties may prevent the encoding of auditory information at high stimulation rates. In the present study, we compare the temporal resolution of light-evoked responses of ChR2 to a recently developed fast opsin, Chronos, to ChR2 in a murine ABI model. Viral mediated gene transfer via a posterolateral craniotomy was used to express Chronos or ChR2 in the cochlear nucleus (CN). Following a four to eight week incubation period, blue light (473 nm) was delivered via an optical fiber placed directly on the surface of the infected CN, and neural activity was recorded in the contralateral inferior colliculus (IC). Both ChR2 and Chronos evoked sustained responses to all stimuli, even at high pulse rates. In addition, optical stimulation evoked excitatory responses throughout the tonotopic axis of the IC. Synchrony of the light-evoked response to stimulus rates of 14–448 pulses/s was higher in Chronos compared to ChR2 mice ($p < 0.05$ at 56, 168, and 224 pulses/s). Our results demonstrate that Chronos has the ability to drive the auditory system at higher stimulation rates than ChR2 and may be a more ideal opsin for manipulation of auditory pathways in future optogenetic-based neuroprostheses.

This article is part of a Special Issue entitled "Lasker Award".

1. Introduction

The cochlear implant (CI) is the most successful of neuroprostheses, and provides meaningful auditory benefits to pediatric and adult patients with severe to profound hearing loss. In the past 50 years, over 300,000 individuals worldwide have received a CI (NIDCD, 2014). Over this period, CI technology has evolved from a crude single channel implant to a multi-channel auditory neurostimulator providing sound and speech perception to the majority of deaf users. Cochlear implants have proven highly beneficial for several etiologies of hearing loss, including genetic causes of deafness (Vivero et al., 2010). The recent Lasker Award highlights the development of the CI and illustrates the profound success of this device and its positive impact on society (Williams, 2013). However, there is a small subset of deaf individuals who will not benefit from the CI due to 1) a small or absent cochlea, 2) a small or absent auditory nerve, or 3) injury or scarring of the inner ear or auditory nerve secondary to meningitis, trauma, or tumor, such as bilateral vestibular schwannomas that arise from Neurofibromatosis-2 (NF-2) (Asthagiri et al., 2009). An auditory brainstem implant (ABI) is an option to provide hearing sensations in these patients who are not candidates for the CI due to these considerations. More than 1000 patients worldwide have been implanted with an ABI (Lin et al., 2012). The ABI bypasses the

* Corresponding author. Wilson Auditory Brainstem Implant Program, Massachusetts Eye and Ear Infirmary, Department of Otology and Laryngology, Harvard Medical School, 243 Charles Street, Boston, MA 02114, USA.
E-mail address: Daniel_Lee@meei.harvard.edu (D.J. Lee).
[1] Contributed equally.

http://dx.doi.org/10.1016/j.heares.2015.01.004
0378-5955/

damaged or absent cochlea and auditory nerve to transmit electrical stimuli to the cochlear nucleus (CN) in the brainstem (Hitselberger et al., 1984; Sennaroglu et al., 2009).

Hearing outcomes of ABI users are highly variable across similar cohorts of patients (Colletti et al., 2012; Colletti and Shannon, 2005; Nevison et al., 2002), and overall performance of ABI users lags behind that seen for CI users. Further, many ABI users experience side effects, such as facial pain, tingling, and twitching, as well as dizziness, due to activation of non-auditory neurons (Colletti et al., 2010). One possible explanation for limited outcomes and side effects may be the spread of electric current (Eisen and Franck, 2005; Nardo et al., 2008; Venter and Hanekom, 2014). One approach to improve speech perception is to increase the number of electrode channels. However, due to current spread, this may result in channel cross talk (Boëx et al., 2003; Karg et al., 2013; Qazi et al., 2013).

Optical stimulation of the nervous system is now being used as a novel stimulus paradigm in research laboratories. For the central auditory system, light-based activation offers a theoretical advantage over traditional electric-based neural stimulation as focused light may be able to excite a select set of neurons, increasing the density of independent stimulation channels while reducing the unintended consequence of current spread (Fu and Nogaki, 2005; Fu et al., 1998). These properties could address the limitations seen with the electrically based ABI. Over the past decade, infrared neural stimulation (INS) of the auditory system has been investigated as an alternative means to stimulate neurons; however, INS may have limited applications in the central auditory system. Recent efforts employing INS in the central auditory system have failed to elicit an evoked response in a deafened animal model, limiting its potential clinical utility (Verma et al., 2014).

In contrast to INS, optogenetics uses light from the visible spectrum to stimulate the nervous system, and it has been used to investigate a host of neural systems (Ayling et al., 2009; Boyden et al., 2005; Huff et al., 2013; Rolls et al., 2011). Viral-mediated infection is a common approach to deliver genes encoding for microbial opsins, light-gated transmembrane channels that enable neurons to respond to optical stimulation. ChR2 is the most widely used opsin in neuroscience (Bernstein et al., 2008; Boyden et al., 2005; Chow et al., 2010; Han and Boyden, 2007; Zhang et al., 2006), however, only a few recent studies have applied optogenetics to the auditory system (Hernandez et al., 2014; Shimano et al., 2013). Shimano et al. introduced ChR2 into the CN and demonstrated light-evoked increases in auditory neural activity locally in the CN. Building on the results of Shimano et al., we previously showed optogenetic stimulation of the CN results in activation of the auditory pathway, including the inferior colliculus and auditory cortex (Darrow et al., 2014). In a recent optogenetics study of the peripheral auditory system, transgenic mice expressing ChR2 in spiral ganglion neurons (SGN) of the cochlea showed neural responses in SGNs themselves and CN and the in neurons of the central auditory pathway (IC) (Hernandez et al., 2014). Overall, these studies demonstrate that optogenetics can be used to activate the auditory system from the periphery throughout the central pathway.

One unique property of the auditory system is its capability of providing a highly synchronous response with the rapidly varying features of an acoustic waveform, a property necessary to encode the also rapidly varying characteristics of speech. Original studies of the kinetics of ChR2 and its variants (Boyden et al., 2005; Zhang et al., 2006) suggest that ChR2 may be too slow for optimal function in the auditory system (Darrow et al., 2014). Over the last several years, a host of new opsins have become available with variable activation thresholds, wavelengths of stimulation, and most importantly, kinetic properties (Yizhar et al., 2011). One of the most recently developed opsins, Chronos (Klapoetke et al., 2014), appears to have faster kinetic properties that may be better suited for conveying temporal cues to the auditory system. Herein, we compare the temporal characteristics of ChR2 and Chronos in a translational murine ABI model.

2. Methods

2.1. Animal protocol

All experimental procedures were performed in accordance with the National Institutes of Health guidelines for the care and use of laboratory animals as well as the approved animal care and use protocols at the Massachusetts Eye & Ear Infirmary, Boston, MA.

2.2. Surgical exposure of the dorsal cochlear nucleus

Methods to expose the dorsal cochlear nucleus (DCN) have been described (Kozin et al., 2015). Direct exposure of the DCN, rather than stereotaxic injection, was used to minimize the chances of missing the desired injection site in addition to replicating the potential surgical approach used during human ABI operations. Normal hearing CBA/CaJ mice aged 4–6 weeks were anesthetized with xylazine (10 mg/kg) and ketamine (100 mg/kg) via an intraperitoneal (IP) administration. Following anesthesia, the overlying scalp was exposed to provide unobstructed access to the surgical site. The mouse was placed in a Kopf small animal stereotaxic holder (Tujunga, CA), and held in place by a snout clamp. The left parietal, interparietal, and occipital bones of the skull are exposed and rongeurs are used to make a craniotomy over the interparietal bone, left of midline, ~2 mm caudal to the lambda suture line. Following craniotomy, using a 5 French suction, aspiration of lateral-most portion of the left cerebellum reveals the underlying DCN (Fig. 1).

2.3. Pressure microinjection for gene transfer

After the DCN was clearly visible, pressure microinjections are made into the DCN using a 5 μl Hamilton syringe. Between 1.5 and 2.0 μl of adeno-associated virus with ChR2 (AAV2.8-ChR2 fused with GFP or mCherry and CAG promoter, courtesy of Dr. Edward Boyden's lab) or Chronos (AAV 2/8) were infused over a 2–4 min period. (Plasmid for Chronos was provided by Dr. Edward Boyden, Massachusetts Institute of Technology, Cambridge, MA. Amplification took place at the Boston Children's Viral Core, Boston, MA. Measured titers of Chronos were 1.21×10^{14} GC/ml.) Immediately following injection, the incision was closed and the scalp was sutured. Four additional mice were used as either 'sham' or control cases. These included sham-injected mice ($n = 2$) that underwent the exact surgical protocol as AAV injected mice, including injection of saline into the brainstem over 2–4 min, and control mice ($n = 2$), which had no history of manipulation.

2.4. Re-exposure of dorsal cochlear nucleus and exposure of contralateral inferior colliculus

After a four to eight week survival time to allow expression of either ChR2 or Chronos, the mice were prepared for acute surgery to characterize responses to optical stimulation. Mice were re-anesthetized and underwent the above-described surgical procedure for performing the craniotomy and the cerebellar aspiration for direct visualization of the DCN. After the injected region was re-exposed for optical stimulation, a craniotomy was made over the right IC and the exposed brain surface was covered with high-viscosity silicon oil. During the course of physiological recordings,

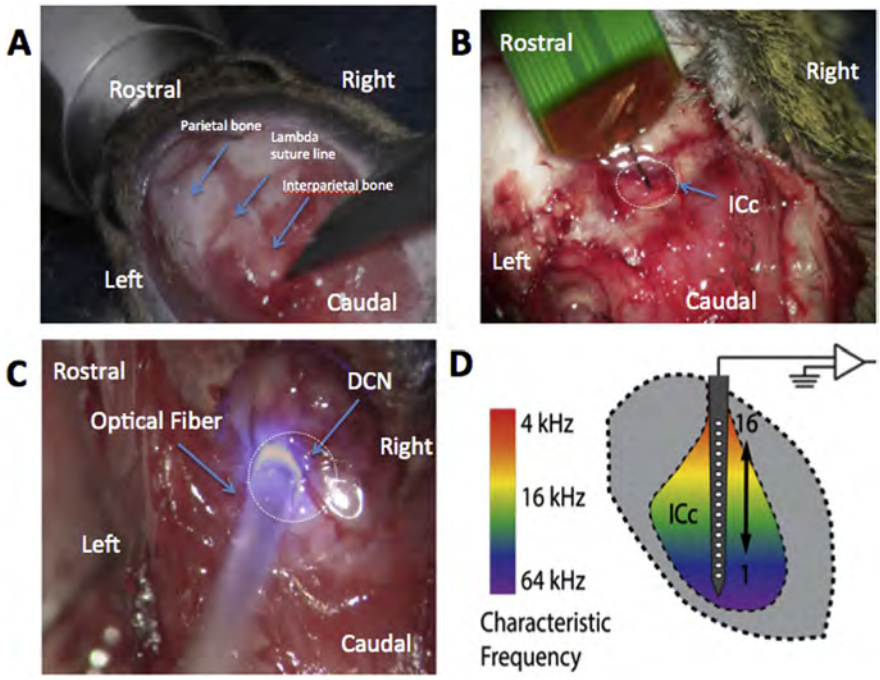

Fig. 1. Surgical approach to the DCN for opsin injection and IC for neural recording with a multichannel electrode probe. A: The skin and muscle are retracted laterally to expose the lambda and the coronal suture lines. B: Placement of NeuroNexus recording probe into the IC in a vertical direction. C: Left-sided posterior craniotomy and partial cerebellar aspiration have been performed and a 400 μm diameter optical fiber mounted on a micromanipulator is introduced through the craniotomy and onto the CN surface. D: Schematic representation of the recording probe positioned along the tonotopic axis of the central nucleus of the inferior colliculus (ICc) so that each of the 16 recording electrodes (spaced 50 μm apart) records a different characteristic frequency.

the core body temperature of the animal was maintained at 36.8 °C with a homeothermic blanket system.

2.5. Optical stimulation

Blue light (473 nm) stimuli were produced by a laser (BL473T-100FC, Shanghai Laser & Optics Century Co.) targeting the peak wavelength sensitivities of ChR2 (~475 nm) and Chronos (~500 nm) (Klapoetke et al., 2014). Light stimuli were delivered via an optical fiber (400 μm diameter) that was held in place by a micromanipulator and placed directly on the exposed surface of the DCN (Fig. 1). Pulses of 1 ms duration were presented at pseudo-randomized rates from 14 to 448 pulses/s for train durations of 300 or 500 ms followed by 300 or 500 ms of no stimulation, respectively. Either 50 or 80 trials were presented at light intensity ranging from 0 to 13 mW. The laser was calibrated by positioning the 400 μm diameter optical fiber ~2 mm from a standard Si photodiode power sensor (9.5 mm diameter, Thorlabs S121C) connected to a USB power and energy meter interface (Thorlabs PM100USB). The voltage command parameters were systematically varied based on the range of pulse amplitudes, widths, and rates used experimentally. Resulting measured laser intensity (radiant exposure, mW) was calibrated to the voltage input.

2.6. Contralateral inferior colliculus recordings

Multiunit recordings were made from the central nucleus of the IC using a penetrating 16-channel linear silicone probe (NeuroNexus Technologies, Fig. 1). The position of the recording probe was first inserted perpendicular to the exposed surface above the IC, approximately ~1 mm lateral to the midline and immediately caudal to the transverse sinus. The probe was repositioned until a complete tonotopic map across the recording channels was obtained (Guo et al., 2012; Malmierca et al., 1993) using acoustic frequencies from 8 to 45.25 kHz in 0.5 octave steps and from 0 to 80 dB in 10 dB steps, using 20 ms duration tone bursts with a repetition rate of 10 bursts/s. Injected mice had acoustic thresholds (<40 dB SPL) comparable to non-injected mice. Raw voltage signals were band-pass filtered (0.3–3 kHz, 5 pole) and sampled at 25 kHz. Common mode rejection was performed across all 16 channels and then the signal was digitally filtered (zero-phase butterworth band-pass filter, 0.5–3 kHz, 5-pole).

To compute driven firing rate, average spike count was computed over the pulse train duration and spontaneous firing rate, computed from spikes collected during the no stimulation period, was subtracted from it. Paired *t*-tests were performed between the firing rates and spontaneous rates from every trial for each electrode and stimulus intensity. For each electrode-intensity combination in which the driven rate was not significant ($p > 0.01$), the driven rate was assigned to be 0 spikes/second. Driven rate–intensity curves were generated from the average of driven rate across all electrodes collected during each stimulus intensity presented at 28 pulses/s and normalized to the highest driven rate evoked by any stimulus intensity. To investigate temporal properties of laser-evoked spiking we computed the synchronization index (SI, magnitude of the vector of averaged spikes collected during the period between stimulus pulses; the SI varies between 0 (no synchronization) and 1 (all spikes occurring exactly at the same phase of the stimulus period); Dynes and Delgutte, 1992). For all stimulus electrode-intensities in which driven rate was calculated to be zero spikes/s SI was also set to zero.

2.7. Histology and immunohistochemistry

Following conclusion of experiments, mice were euthanized with an overdose of ketamine and perfused with normal saline followed by 4% paraformaldehyde. Brainstems were extracted from

the skull and post-fixed for 2 h. Brainstems were cryoprotected in 30% sucrose for 48 h, and then sectioned using a cryostat into 30–60 μm sections. Before the staining procedure, sections were allowed to thaw at room temperature and then rehydrated in PBS for 10 min. After washing with PBS, tissue was permeabilized and blocked with blocking solution (0.3% Triton X-100, 15% heat inactivated goat or donkey serum in PBS) for 1 h. Visualization of cell nuclei was enabled with 4,6-diamidino-2-phenylindole (DAPI; Vector Laboratories). Staining was analyzed with epifluorescence microscopy (Axioskop2 Mot Axiocam, Zeiss) and confocal microscopy (Leica).

3. Results

3.1. Expression of Chronos and ChR2 in the cochlear nucleus

Opsin-linked immunofluorescence demonstrated Chronos or ChR2 gene transfer throughout the DCN and in the ventral cochlear nucleus (VCN). Chronos-GFP immunofluorescence appeared in an array of cell types, including morphologies consistent with DCN fusiform cells (red arrow, Fig. 2B), giant cells, and cartwheel cells. We did not directly investigate anterograde labeling of axons in Chronos cases, but such labeling has been observed previously in ChR2 cases, which employed an identical AAV serotype and promoter (Darrow et al., 2014).

3.2. Synchronization and driven rate of IC neural activity in response to optical stimulation of CN

Neural activation in the IC was evoked by light stimulation of the CN. Dot raster and peristimulus time (PST) histogram plots from one recording site in a Chronos mouse are shown in Fig. 3. High, sustained rates of firing were observed during the light pulse trains and low rates of spontaneous firing were observed when there are no stimuli (second half of traces). For the pulse train of 448 pulses/s (Fig. 3B), the PST histogram shows that the high initial firing adapted to steady-state firing over the course of the 500-ms pulse train. Even during the adapted portion of the evoked response, the driven rates were sustained and above spontaneous firing. This adaptation was not present for the low pulse rate (Fig. 3A), even though the overall firing rate was slightly lower.

The temporal pattern of evoked neural activity in the IC depends on the stimulus pulse rate. For the train of pulses at 28 pulses/s (Fig. 3A), evoked activity was synchronized to the pulses, whereas for the train of pulses at 448 pulses/s (Fig. 3B), evoked activity, though high, appeared to be less synchronized. The average SI values are plotted against stimulus rate for Chronos and ChR2 cases in Fig. 4A. For both opsins, there was a decline in SI with increasing pulse rate. For all rates, recordings from Chronos mice had higher SI than those from ChR2 mice. These differences were significant at rates of 56, 168 and 224 pulses/s (Fig. 4A, asterisks).

The decline in synchrony with increasing pulse rate was not due to a decline in firing rate and driven rate was significant at all tested stimulus rates (14–448 pulses/s, Fig. 4B). Even at high pulse rates (e.g. 448 pulses/s), evoked activity was significantly above spontaneous (paired *t*-test), high (average 76 spikes/s), and sustained over the entire stimulus pulse train (Fig. 3B) despite the compromised kinetics of both Chronos and ChR2. Further, the firing rates of mice injected with Chronos or ChR-2 were increasing, monotonic functions of laser intensity, with evidence of incomplete saturation at the highest tested intensities (Fig. 5A). At these intensities, average firing rates were significantly lower ($p < 0.001$) for ChR2 versus Chronos, average rate 55 spikes/s for ChR2 versus 127 spikes/s for Chronos (~12 mW, stimulus rate = 28 pulses/s).

3.3. Spatial pattern of response for optogenetic-based stimulation of the cochlear nucleus

There was variability in the spatial pattern of responses from case to case. Fig. 5B shows a case where nearly all electrodes recorded laser-evoked activity for stimulus levels at and above threshold (driven rate > 0 spikes/s, indicated by non-dark blue coloring, in the web version). Highest spike rates were observed on electrodes 2–8. Other cases (data not shown) had variable patterns of neural activation: of the 16 electrodes, the average number activated across all laser intensities at and above threshold (stimulus rate = 28 pulses/s) was 12.4 with a range of 9–14.9 electrodes for Chronos ($n = 4$ mice) and 9.2 with a range of 4.6–14 electrodes for ChR2 ($n = 4$ mice). Our data set is insufficient, though, to correlate the opsin staining pattern with the spatial pattern of responses. Sham and control mice showed no response to optical stimulation (one example shown in Fig. 5C).

4. Discussion

4.1. Chronos versus ChR2 for light-evoked activation of the auditory system

Our study is the first to characterize the temporal properties of opsins expressed in the central auditory system. Of all presently studied opsins, Chronos has the fastest on/off kinetics based on

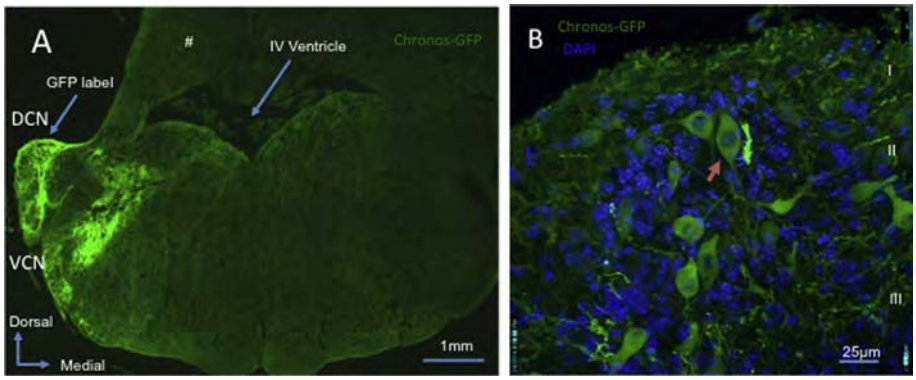

Fig. 2. Chronos expression in the cochlear nucleus. A: Mosaic confocal image showing Chronos-GFP expression within the dorsal cochlear nucleus (DCN) and ventral cochlear nucleus (VCN). B: Confocal image of the DCN demonstrates Chronos-GFP expression within a fusiform cell (red arrow) and in other neuronal populations. DAPI demonstrates cell nuclei. (For interpretation of the references to color in this figure legend, the reader is referred to the web version of this article.)

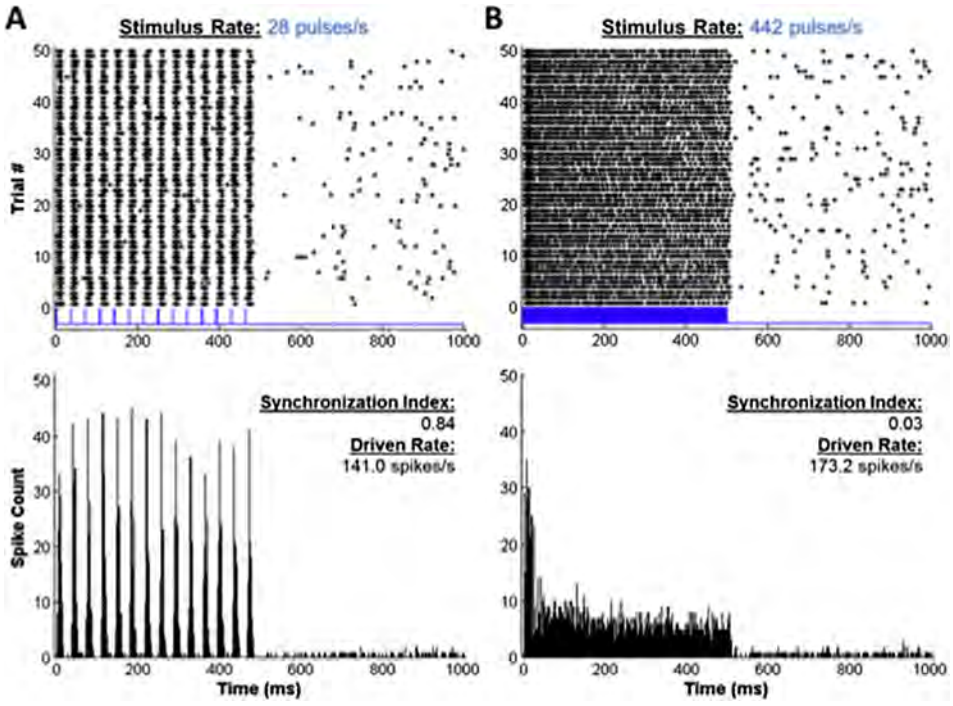

Fig. 3. IC neural activity evoked by light pulses (Chronos injected mouse). A: Responses at a low stimulus rate (28 pulses/s) elicit synchronized spikes (dots on raster plot at top). Bottom plot shows PST histogram for the same data. B: Responses at a high stimulus rate (448 pulses/s) show less synchrony (synchronization index indicated on the plots). In addition, the PST histogram shows the prominent rate adaptation during the pulse train. Driven rates (an average over the 500 ms duration pulse train) are indicated on the plots.

firing rates in *in vitro* studies (Klapoetke et al., 2014). For *in vivo* stimulation of the CN, we found that the use of Chronos resulted in better neural synchrony to light stimuli compared to ChR2. For both opsins, there was a decline in SI with increasing pulse rates; however, the decline was more pronounced for ChR2. Significant differences in the SI of evoked activity between the two opsins were found at 56, 168 and 224 pulses/s. Synchronous activity at these pulse rates are clinically significant because contemporary clinical ABI processors employing the SPEAK sound processing strategy use pulse rates of 250 pulses/s; this pulse rate is a carrier that works well for neural encoding of amplitude modulation (McCreery et al., 2013).

Although the temporal properties of optogenetic responses have not been characterized previously, the responses of IC neurons to electrical stimulation of the cochlea have previously been reported. These responses also decline with increasing pulse rates, and their synchrony measures are comparable to the optogenetic responses reported here (Middlebrooks and Snyder, 2010; Snyder et al., 1995). In addition, synchrony is even higher in IC recordings from awake animals under comparable stimulus conditions (Chung et al., 2014). In those studies, differences among types of units were observed, with some units able to fire synchronously to high rates (>100 pulses/s) whereas others unable to synchronize to these rates. In the present study, single recording sites probably sampled from a combination of these unit types, future studies could employ spike sorting to examine the synchronization limit of single units to optical stimulation.

During optogenetic stimulation, even for pulse rates for which responses were non-synchronized, driven rates were substantial (Figs. 3B, 4B). Such driven rates will signal the presence of a stimulus even though there is little synchrony to the fine time structure of the stimulus. Further, since rate–intensity curves (Fig. 5B) suggest that the entire dynamic range of the response was not captured due to the limitations of our laser, a higher-intensity stimulus would likely produce even higher driven rates. However, the level at which potential light-induced damage is manifested is not clear.

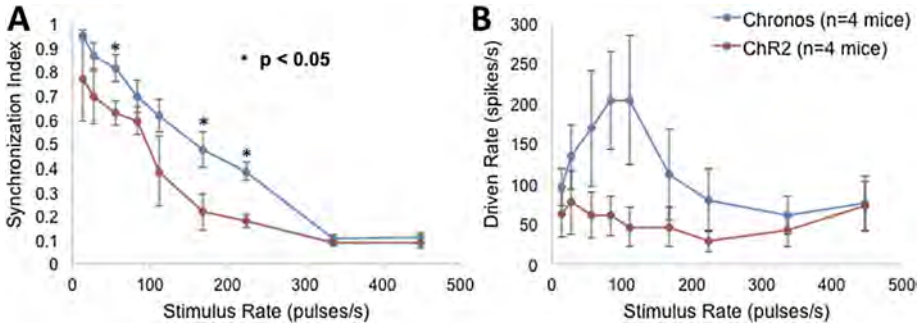

Fig. 4. Synchronization index and driven rate as a function of pulse rate. A: Average SI (at ~12 mW) is significantly greater for Chronos than ChR2 at stimulus rates of 56, 168 and 224 pulses/s (* = $p < 0.05$, two-sample t-test). B: Average maximal driven rates over all 16 electrodes.

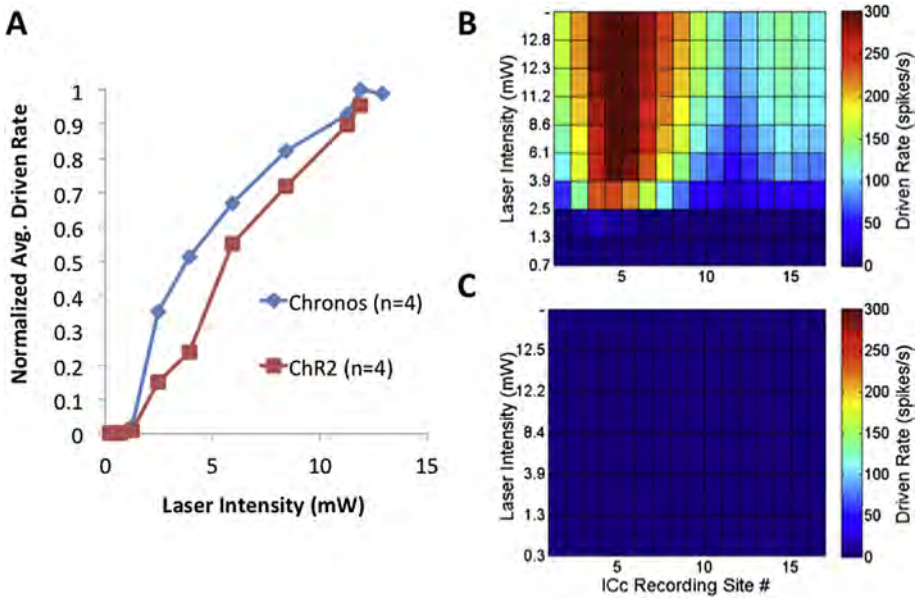

Fig. 5. Neural activity as a function of stimulus intensity and recording position. A: Plot of normalized driven rate across all electrodes as a function of laser intensity for the two opsins. (Stimulus rate = 28 pulses/s). B: Response map showing driven rate as a function of electrode number (position in IC, see Fig. 1D) and laser intensity. (Chronos injected mouse, stimulus rate = 56 pulses/s.) C: Control mouse response map showing no response evoked by light. (Stimulus rate = 28 pulses/s.)

4.2. Limitations of viral-mediated gene transfer

There are inherent limitations to viral mediated gene transfer in the central nervous system that may have influenced our results. We previously demonstrated that expression of opsins as a result of gene transfer is variable from case to case (Darrow et al., 2014). Consequently, the locations and numbers of activated cells differed somewhat between Chronos and ChR2 cases. This may affect synchrony because, at least for responses to acoustic stimuli, different types of neurons have different temporal characteristics (Young, 1984). We believe that at least some of the excitatory responses observed here may have been mediated by fusiform cells of the DCN because in almost all cases they express Chronos or ChR2 and because they project directly to the IC (Darrow et al., 2014; Oliver, 1984; Oliver and Morest, 1984). Perhaps the slow kinetics of ChR2 in these cells accounts for both the low SI and lower driven rates observed in our study. Regardless of the exact etiology, the performance of Chronos is superior in both driven rate and SI.

4.3. Translational models and future optogenetics research in the central auditory system

In addition to examining the temporal properties of Chronos and ChR2, our study demonstrates a feasible translational approach for gene transfer of opsins to the CN. Specifically, our surgical approach in the murine model allows for visualization of the DCN and inoculation with a viral gene transcript (Kozin et al., 2015). In many respects, our model is analogous to surgical approach of the human ABI placement. While viral mediated gene transfer has inherent weaknesses and risks, numerous FDA-approved gene therapy studies are ongoing and may be a potential tool for gene transfer to the CN of humans.

Further, our study represents the beginning of a path toward the particular opsin chosen for an eventual prosthesis. We define the ideal characteristics of an “auditory opsin” for use in a neuroprosthesis: 1) fast temporal kinetics to encode speech information, 2) low activation threshold to decrease energy requirements from illumination powered by an external source, and 3) a promoter that enables tissue-specificity using virally-mediated gene transduction to the CN (to minimize non-specific expression of opsins). Looking forward, our study raises several questions: What is the ideal gene transfer approach for delivery of opsins to the auditory system? What is the long-term safety profile of opsins, and will there be any deleterious effects from their presence? Finally, can optogenetic-based stimulation function as replacement to electrical stimulation, and can it be used as an adjunct? The answers to these questions, both in the central and peripheral auditory systems, remain to be seen and should be the focus of future studies.

5. Conclusion

Previous studies have demonstrated the feasibility of optogenetic stimulation for light-based activation of the central auditory system. Currently, the most widely used opsin in neuroscience is ChR2; however, it may not possess the temporal properties necessary to encode auditory information. We find, in an ABI animal model, that Chronos has significantly improved kinetic properties compared to ChR2. These studies highlight the need to further examine and identify the ideal opsins that can support the high stimulation rates needed for the transfer of temporal cues along the auditory pathways. Future studies may seek to design opsins optimized for a new generation ABI based on light.

Acknowledgments

Preliminary results of this study were presented at the Association for Research in Otolaryngology Midwinter Meeting, February 2013 and 2014. This work was supported by a Fondation Bertarelli grant (DJL and MCB), a MED-EL grant (DJL), and National Institutes of Health Grants DC01089 (MCB), T32 DC000038 (AEH), T32 DC000020 (EDK).

References

Asthagiri, A., Parry, D., Butman, J., Kim, H., Tsilou, E., Zhuang, Z., Lonser, R., 2009. Neurofibomatosis type 2. Lancet 373, 1974–1986.

Ayling, O.G., Harrison, T.C., Boyd, J.D., Goroshkov, A., Murphy, T.H., 2009. Automated light-based mapping of motor cortex by photoactivation of channelrhodopsin-2 transgenic mice. Nat. Methods 6, 219–224.

Bernstein, J.G., Han, X., Henninger, M.A., Ko, E.Y., Qian, X., Franzesi, G.T., McConnell, J.P., Stern, P., Desimone, R., Boyden, E.S., 2008. Prosthetic systems for therapeutic optical activation and silencing of genetically-targeted neurons. Proc. Soc. Photo Opt. Instrum. Eng. 6854, 68540H.

Boëx, C., de Balthasar, C., Kós, M.-I., Pelizzone, M., 2003. Electrical field interactions in different cochlear implant systems. J. Acoust. Soc. Am. 114, 2049.

Boyden, E.S., Zhang, F., Bamberg, E., Nagel, G., Deisseroth, K., 2005. Millisecond-timescale, genetically targeted optical control of neural activity. Nat. Neurosci. 8, 1263–1268.

Chow, B.Y., Han, X., Dobry, A.S., Qian, X., Chuong, A.S., Li, M., Henninger, M.A., Belfort, G.M., Lin, Y., Monahan, P.E., Boyden, E.S., 2010. High-performance genetically targetable optical neural silencing by light-driven proton pumps. Nature 463, 98–102.

Chung, Y., Hancock, K.E., Nam, S.I., Delgutte, B., 2014. Coding of electric pulse trains presented through cochlear implants in the auditory midbrain of awake rabbit: comparison with anesthetized preparations. J. Neurosci. 34, 218–231.

Colletti, L., Shannon, R., Colletti, V., 2012. Auditory brainstem implants for neurofibromatosis type 2. Curr. Opin. Otolaryngol. Head Neck Surg. 20, 353–357.

Colletti, V., Shannon, R.V., 2005. Open set speech perception with auditory brainstem implant? Laryngoscope 115, 1974–1978.

Colletti, V., Shannon, R., Carner, M., Veronese, S., Colletti, L., 2010. Complications in auditory brainstem implant surgery in adults and children. Otol. Neurotol. 31, 558–564.

Darrow, K.N., Slama, M.C., Kozin, E., Owoc, M., Hancock, K., Kempfle, J., Edge, A., Lacour, S., Boyden, E., Polley, D., Brown, M.C., Lee, D.J., 2014 Dec 3. Optogenetic stimulation of the cochlear nucleus using channelrhodopsin-2 evokes activity in the central auditory pathway. Brain Res. PMID: 25481416.

Dynes, S., Delgutte, B., 1992. Phase-locking of auditory-nerve discharges to sinusoidal electric stimulation of the cochlea. Hear Res. 58, 79–90.

Eisen, M.D., Franck, K.H., 2005. Electrode interaction in pediatric cochlear implant subjects. J. Assoc. Res. Otolaryngol. 6, 160–170.

Fu, Q., Nogaki, G., 2005. Noise susceptibility of cochlear implant users: the role of spectral resolution and smearing. J. Assoc. Res. Otolaryngol. 6, 19–27.

Fu, Q.J., Shannon, R.V., Wang, X., 1998. Effects of noise and spectral resolution on vowel and consonant recognition: acoustic and electric hearing. J. Acoust. Soc. Am. 104, 3586–3596.

Guo, W., Chambers, A., Darrow, K., Hancock, K., Shinn-Cunningham, B., Polley, D., 2012. Robustness of cortical topography across fields, laminae, anesthetic states, and neurophysiological signal types. J. Neurosci. 32, 9159–9172.

Han, X., Boyden, E.S., 2007. Multiple-color optical activation, silencing, and desynchronization of neural activity, with single-spike temporal resolution. PLoS One 2, e299.

Hernandez, V.H., Gehrt, A., Reuter, K., Jing, Z., Jeschke, M., Mendoza Schulz, A., Hoch, G., Bartels, M., Vogt, G., Garnham, C.W., Yawo, H., Fukazawa, Y., Augustine, G.J., Bamberg, E., Kugler, S., Salditt, T., de Hoz, L., Strenzke, N., Moser, T., 2014. Optogenetic stimulation of the auditory pathway. J. Clin. Investig. 124, 1114–1129.

Hitselberger, W., House, W., Edgerton, B., Whitaker, S., 1984. Cochlear nucleus implant. Otolaryngol. Head Neck Surg. 92, 52–54.

Huff, M.L., Miller, R.L., Deisseroth, K., Moorman, D.E., LaLumiere, R.T., 2013. Post-training optogenetic manipulations of basolateral amygdala activity modulate consolidation of inhibitory avoidance memory in rats. Proc. Natl. Acad. Sci. U. S. A. 110, 3597–3602.

Karg, S., Lackner, C., Hemmert, W., 2013. Temporal interaction in electrical hearing elucidates auditory nerve dynamics in humans. Hear Res. 299, 10–18.

Klapoetke, N.C., Murata, Y., Kim, S.S., Pulver, S.R., Birdsey-Benson, A., Cho, Y.K., Morimoto, T.K., Chuong, A.S., Carpenter, E.J., Tian, Z., Wang, J., Xie, Y., Yan, Z., Zhang, Y., Chow, B.Y., Surek, B., Melkonian, M., Jayaraman, V., Constantine-Paton, M., Wong, G.K., Boyden, E.S., 2014. Independent optical excitation of distinct neural populations. Nat. Methods 11, 338–346.

Kozin, E., Darrow, K., Hight, A., Lehmann, A., Kaplan, A., Brown, M., Lee, D., 1/20/2015. Direct visualization of the murine dorsal cochlear nucleus for optogenetic stimulation of the auditory pathway. JoVE 95. http://dx.doi.org/10.3791/52426.

Lin, H., Herrmann, B., Lee, D., 2012. Auditory Brainstem Implants. Plural Publishing, San Diego.

Malmierca, M.S., Blackstad, T.W., Osen, K.K., Karagulle, T., Molowny, R.L., 1993. The central nucleus of the inferior colliculus in rat: a Golgi and computer reconstruction study of neuronal and laminar structure. J. Comp. Neurol. 333, 1–27.

McCreery, D., Han, M., Pikov, V., Yadav, K., Pannu, S., 2013. Encoding of the amplitude modulation of pulsatile electrical stimulation in the feline cochlear nucleus by neurons in the inferior colliculus; effects of stimulus pulse rate. J. Neural Eng. 10, 056010.

Middlebrooks, J.C., Snyder, R.L., 2010. Selective electrical stimulation of the auditory nerve activates a pathway specialized for high temporal acuity. J. Neurosci. 30, 1937–1946.

Nardo, W.D., Cantore, I., Marchese, M.R., Cianfrone, F., Scorpecci, A., Giannantonio, S., Paludetti, G., 2008. Electric to acoustic pitch matching: a possible way to improve individual cochlear implant fitting. Eur. Arch. Otorhinolaryngol. 265, 1321–1328.

Nevison, B., Laszig, R., Sollmann, W., Lenarz, T., Sterkers, O., Ramsden, R., Fraysse, B., Manrique, M., Rask-Andersen, H., Garcia-Ibanez, E., Colletti, V., von Wallenberg, E., 2002. Results from a European clinical investigation of the nucleus multichannel auditory brainstem implant. Ear Hear 23, 170–183.

NIDCD, 2014. Cochlear Implants [Online]. http://wwwnidcdnihgov/health/hearing/pages/cochaspx (verified 08.18.14.).

Oliver, D.L., 1984. Dorsal cochlear nucleus projections to the inferior colliculus in the cat: a light and electron microscopic study. J. Comp. Neurol. 224, 155–172.

Oliver, D.L., Morest, D.K., 1984. The central nucleus of the inferior colliculus in the cat. J. Comp. Neurol. 222, 237–264.

Qazi, O., van Dijk, B., Moonen, M., Wouters, J., 2013. Understanding the effect of noise on electrical stimulation sequences in cochlear implants and its impact on speech intelligibility. Hear Res. 299, 79–87.

Rolls, A., Colas, D., Adamantidis, A., Carter, M., Lanre-Amos, T., Heller, H.C., de Lecea, L., 2011. Optogenetic disruption of sleep continuity impairs memory consolidation. Proc. Natl. Acad. Sci. U. S. A. 108, 13305–13310.

Sennaroglu, L., Ziyal, I., Atas, A., Sennaroglu, G., Yucel, E., Sevinc, S., Ekin, M., Sarac, S., Atay, G., Ozgen, B., Ozcan, O., Belgin, E., Colletti, V., Turan, E., 2009. Preliminary results of auditory brainstem implantation in prelingually deaf children with inner ear malformations including severe stenosis of the cochlear aperture and aplasia of the cochlear nerve. Otol. Neurotol. 30, 708–715.

Shimano, T., Fyk-Kolodziej, B., Mirza, N., Asako, M., Tomoda, K., Bledsoe, S., Pan, Z.H., Molitor, S., Holt, A.G., 2013. Assessment of the AAV-mediated expression of channelrhodopsin-2 and halorhodopsin in brainstem neurons mediating auditory signaling. Brain Res. 1511, 138–152.

Snyder, R., Leake, P., Rebscher, S., Beitel, R., 1995. Temporal resolution of neurons in cat inferior colliculus to intracochlear electrical stimulation – effects of neonatal deafening and chronic stimulation. J. Neurophysiol. 73, 449–467.

Venter, P., Hanekom, J., 2014 Oct. Is there a fundamental 300 Hz limit to pulse rate discrimination in cochlear implants? J. Assoc. Res. Otolaryngol. 15 (5), 849–866.

Verma, R.U., Guex, A.A., Hancock, K.E., Durakovic, N., McKay, C.M., Slama, M.C., Brown, M.C., Lee, D.J., 2014. Auditory responses to electric and infrared neural stimulation of the rat cochlear nucleus. Hear Res. 310, 69–75.

Vivero, R.J., Fan, K., Angeli, S., Balkany, T.J., Liu, X.Z., 2010. Cochlear implantation in common forms of genetic deafness. Int. J. Pediatr. Otorhinolaryngol. 74, 1107–1112.

Williams, C., 2013. Hearing restoration: Graeme Clark, Ingeborg Hochmair, and Blake Wilson receive the 2013 Lasker~DeBakey Clinical Medical Research Award. J. Clin. Invest 123, 4102–4106.

Yizhar, O., Fenno, L.E., Davidson, T.J., Mogri, M., Deisseroth, K., 2011. Optogenetics in neural systems. Neuron 71, 9–34.

Young, E.D., 1984. Response characteristics of neurons of the cochlear nuclei. In: Berlin, C.I. (Ed.), Hearing Science: Recent Advances. College-Hill Press, San Diego, pp. 423–460.

Zhang, F., Wang, L.P., Boyden, E.S., Deisseroth, K., 2006. Channelrhodopsin-2 and optical control of excitable cells. Nat. Methods 3, 785–792.